IJMF, Iranian Journal of Materials Forming, Vol. 2, No. 1, pp 30-42
Printed in The Islamic Republic of Iran, 2015

Hot and Cold Tensile Behavior of Al 6061 Produced By Equal Channel Angular Pressing and Subsequent Cold Rolling

A.A. Khamei*[1] K. Dehghani,[1] S. Bakhshi[2] and K. Kalayeh[3]

[1]Department of Mining and Metallurgical Engineering, Amirkabir University of Technology, Tehran, Iran
[2]Metallic Materials Research Center (MMRC-MA), Malkashtar University, Tehran, Iran
[3]Department of Mechanical Engineering, University of Maryland, Baltimore County, USA

Abstract: The full annealing AA6061 aluminum alloy was subjected to severe plastic deformation via the combination of equal channel angular pressing (ECAP) and cold rolling (CR) in order to refine its microstructure and to improve its mechanical properties. According to the results of hot and cold tensile tests, the combination of ECAP and CR significantly affected the final strength and ductility of studied AA6061. Four passes of ECAP followed by 90% reduction in rolling led to about 5.4 and 3.15 times increase in the yield and ultimate tensile strengths, respectively. In addition, the hot ductility and strain rate sensitivity were increased by applying ECAP plus CR. The changes in mechanical properties were attributed to the enhanced dislocation density and to the reduced grain size. The results show that a decrease in grains/subgrains size (0.37 μm) and an increase in the fraction of high angle grain boundaries, exhibited significant effect on the hot ductility of higher severe plastic deformed sample.

Keywords: Severe plastic deformation, Ultrafine-Grain (UFG), 6061 Al alloy, Rolling, Hot ductility

1. Introduction

Recently, different severe plastic deformation (SPD) methods such as high-pressure torsion (HPT), accumulative roll bonding (ARB), equal-channel angular pressing (ECAP), multiple forging (MF), twist extrusion (TE) etc. are widely used to modify the microstructure of materials. Among these techniques, the ECAP process is a promising and interesting method [1]. During the last decade, ECAP has been used as a well-known procedure to fabricate the ultrafine-grained materials and alloys. However, in terms of industrial applications, the dimensions of processed by ECAP products are not large enough [2]. In general, the nanostructured materials produced by SPD offer many superior properties and numerous applications such as in sport equipments, electronic, micro electro-mechanical systems (MEMS), oil, gas, and energy sectors [3], biomedical devices [4], aerospace and transportation industry [5]. On the other hand, aluminum alloys are widely used as the main materials in the automobile, aerospace and construction industries due to their low density, high strength and workability [6]. It is reported that about 46% of aluminum alloys are used in the form of sheets and plates for various applications [7]. Furthermore, the AA6061 aluminum alloy is used extensively in construction and transportation industry because of its good combination of strength and formability [8]. So far, many SPD processes have been used to produce ultrafine grained (UFG) AA6061 [9, 10]. However, there are only a few works concerning the application of ECAP to produce large plates [11-13]. In addition, most ECAP dies are designed to fabricate the small bars with either circular or square cross-sections. Thus, using ECAP, it is difficult to fabricate sheets or plates which are the most required shapes for many industrial applications. To

Received by the editors February 26, 2015; Revised March 25, 2015 and Accepted March 27, 2015.
*Corresponding author (khamei@aut.ac.ir)

overcome the aforementioned deficiencies of ECAP, one practical approach is to combine the ECAP and cold rolling (CR) processes. Using this approach, one is able not only to fabricate the sheets with UFG structure but also to reduce the number of ECAP passes and therefore lowering the costs [14]. As there is a few works regarding the combination of ECAP and CR techniques to produce large strips/sheets of AA6061, the objective of this study is to apply this technique to fabricate the large Ultrafine-Grained sheets. Such products could be readily used in many industries. In addition, the fabricated Ultrafine-Grained sheets with relatively large sizes can be used to study the mechanical properties of Ultrafine-Grained as the there is a shortcoming in preparation of tensile samples, with the sizes and geometries dictated by the standard methods.

2. Materials and Experimental Procedure

The large samples of 100mm×100mm×14 mm made of AA6061-T6 were subjected to ECAP. The composition of studied alloy is mentioned in Table 1.

Table 1. The composition of studied AA-6061 (in wt%).

Sample	Si	Fe	Cu	Mn	Mg	Cr	Al
studied alloy	0.8	0.41	0.21	0.09	0.93	0.09	Bal.
Standard [15]	0.4-0.8	≤0.7	0.15-0.4	≤0.15	0.8-1.2	0.04-0.35	Bal.

Before ECAP, the workpiece was solution treated at 530 ºC for 8 h followed by cooling in furnace. The angles of φ and ψ were 110° and 20°, respectively. Thus, the applied strain per pass was about 0.76 [15]. All the ECAP passes were conducted using route B_{CZ} by rotating the samples 90º around the longitudinal axis between the consecutive passes [16]. Moreover, ECAP processing was performed at room temperature. After the ECAP, the applied cold reduction was about 90%, reaching to the final thickness of 1 mm from 10 mm. The tensile specimens were machined from the processed by ECAP+CR work piece according to the ASTM-E8 [17]. They were prepared along the ECAP and rolling directions. Cold tensile tests were carried out at the strain rate of $4\times10^{-4}s^{-1}$ at ambient temperature. The hot tensile tests were performed at temperature of 673K (400ºC) and at initial strain rates between 5.0×10^{-4}-$1.0\times10^{-2}s^{-1}$. The samples for microstructural observations were prepared using conventional techniques of grinding and mechanical polishing. They were then etched using 6ml HCl + 6ml HF+3ml HNO_3+150ml H_2O solution. The microstructural evolutions were characterized using X-Ray diffraction (XRD) technique, light optical microscopy (LOM) and transmission electron microscopy (TEM) operating at 200kv. The mean grain size was measured by the linear intercept method.

3. Results

3.1. Tensile behavior in room temperature

The engineering stress–strain curves of the Al-6061 alloys before ECAP, after ECAP, and after ECAP+CR are presented in Fig. 1.

In case of processed by ECAP (4passes) sample, the yield strength (YS) and the ultimate tensile strength (UTS) were increased from 63 MPa to 185 MPa and 122 MPa to 216 MPa, respectively. These values are 194% and 77% higher than those of the as-received alloy. The strength of the processed by ECAP alloys differs depending on the number of applied passes. The amounts of uniform elongation were significantly reduced after 4 passes. According to stress-strain curves, the appearance of UTS at very low strains indicates a little work hardening of processed by ECAP specimen. Also, it can be seen from Fig. 1 that the ECAP process resulted in extensive post-necking strain. The work-hardening rate regarding the deformation at different passes of ECAP process decreases sharply with increasing the strain. This is

opposite of the behavior observed regarding the un-deformed sample. In other words, in case of un-deformed sample, the work-hardening rate decreases slowly with increasing the strain so that there is almost a plateau in the work hardening rate. Therefore, this may be one of the reasons why work hardening exponent is decreased with increasing the number of ECAP passes. According to Figure 1, after ECAP+CR, the yield strength and ultimate tensile strength increased significantly from 63 MPa to 340 MPa and 122 MPa to 384 MPa, respectively. These amounts are about 440% and 215% higher than those before ECAP. The strength of double processed by SPD samples, i.e. ECAP+CR, depends on the number of applied passes of either ECAP and/or CR. Although, the elongation was reduced from 24.4% to 3.84% after four passes of ECAP, the ductility was increased 4.11% by applied rolling to processed by ECAP samples. Figure 2 indicates the changes in YS-to-UTS ratio and ductility with increasing the applied plastic strain. According to the past works on the SPD of AA6061, summarized in Table 2, much higher strength than AA6061-T6 can be achieved by the technique presented here. Referring to Table 2, the differences between the mechanical properties obtained by different SPD techniques can be due to the process parameters (e.g. type of deformation, temperature, strain rate, applied strain and route in ECAP etc.), materials characteristics (e.g. initial grain size, SFE etc.), tensile testing conditions (e.g. temperature, strain rate, gauge length, surface quality etc.). Some of aforementioned parameters are mentioned in Table 2.

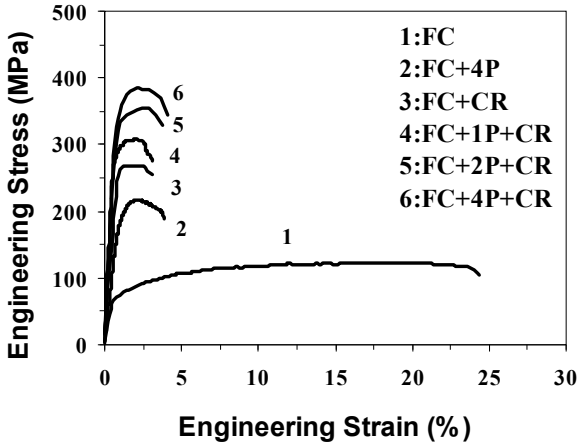

Fig. 1. Stress-Strain curves for the 6061 Al specimens in states furnace cooling (FC), ECAP (P) and ECAP+CR.

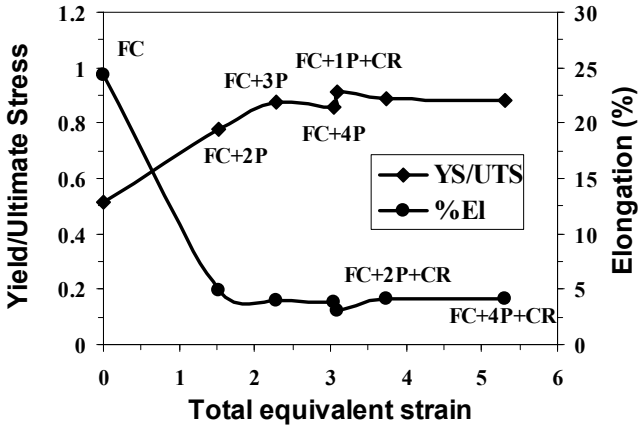

Fig. 2. Variation of yield stress to ultimate tensile stress ratio and elongation with increasing strain in ECAP processing and ECAP+Rolling of 6061Al.

Table 2. A comparison of the properties of SPD-processed AA6061-O (FC: Furnace Cooled) in room temperature.

Severe Plastic Deformation			**Tensile Test**				
Process	**T (°C)**	**ε (%)**	$\dot{\varepsilon}$ **(s^{-1})**	**Gl. (mm)**	**UTS (MPa)**	**YS (MPa)**	**El. (%)**
MAC/F +CR [18]	RT	5.75	1×10^{-4}	10	360	347	-
ECAP [18]	RT	4.2	1×10^{-4}	10	300	280	-
ARB [19]	RT	6.3	8.3×10^{-4}	10	360	-	5
ECAP [20]	RT	6	3.3×10^{-4}	5	305	280	16
ECAP [21]	RT	8	9×10^{-4}	18	340	-	5
ECAP [21]	RT	16	9×10^{-4}	18	300	-	5
HRDSR [22]	120	1.2	5×10^{-4}	5	301	277	6.8
ECAP [23]	70	0.9	5×10^{-4}	10	212	205	18
ECAP [23]	125	0.9	5×10^{-4}	10	208	197	21
ECAP+Rolling [This study]	RT	5.31	4×10^{-4}	31	384	340	4.11

ε : Strain; $\dot{\varepsilon}$: Strain Rate; Gl: Gage Length; UTS: Ultimate Tensile Stress; YS: Yield Stress; El: Elongation to failure; MAC/F: multi-axial compression/forgings; HRDSR: high-ratio differential speed rolling

3.2. Tensile behavior at hot temperature

The typical engineering stress–strain curves of processed by SPD AA6061 deformed at different strain rates (at temperature of 673K) are shown in Fig. 3. Obviously, the flow stress increases quickly with strain in the early stage of deformation, exhibiting a high work-hardening rate. This is followed by a gradual change in the flow stress. For both ECAP+CR and CR cases, the trends are similar, especially at the strain rates of 0.01 and $0.0005s^{-1}$. These curves illustrate that the flow stress rises as the strain rate increases for cases of processed by CR and ECAP (4P) plus CR. At certain strains (peak strain), the flow stress exhibits single peaks which gradually decrease at high strain.

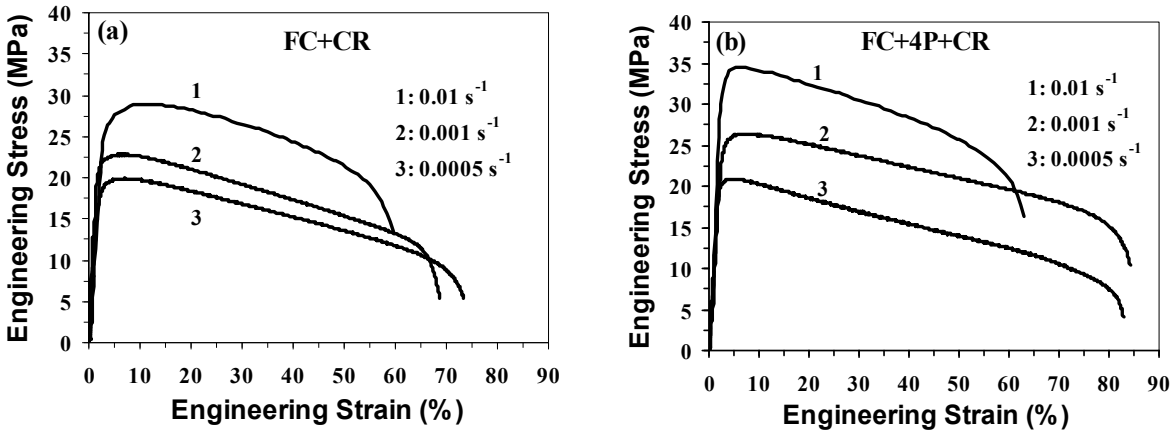

Fig. 3. Flow stress versus elongation to failure over a range of strain rates at 673 K for severe plastic deformed samples: (a) FC+CR and (b) FC+4P+CR.

Strain rate dependences of the hot ductility of the deformed alloy at temperature of 673K are shown in Fig. 4. It is of interest that different SPD methods affect the changes in elongation versus the strain rate. When the workpiece is subjected to only cold rolling, the hot ductility reduces when strain rate increases. However, a peak is observed in the elongation against strain rate for the samples subjected to 4 passes of ECAP+CR. In the other words, the maximum elongation is obtained at the strain rate of $0.001s^{-1}$, and then it decreases with increasing the strain rate. For other conditions (CR and 4P-ECAP), there is no maximum for ductility, and it decreases continuously with increasing strain rate. A similar trend was reported earlier for an Al–Mg–Sc alloy [24] and an Al–Mg alloy [25] for 4-pass ECAP plus cold rolling. It was reported that the trend is differed by increasing the ECAP passes [24].

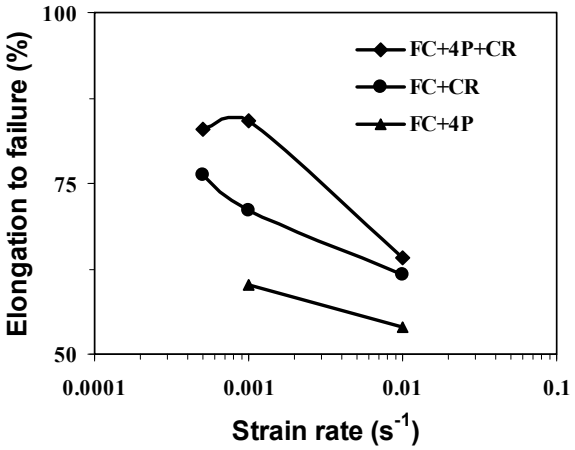

Fig. 4. The changes of elongations to failure against the strain rates.

The variations in the strain rate sensitivity as a function of strain are plotted in Fig. 5. The rate of change in flow stress with strain rate is usually measured as strain rate sensitivity 'm' which is a function of temperature and strain rate. The strain rate sensitivities of the deformed alloy are about 0.1 to 0.15 for FC+CR condition and 0.16 to 0.18 for 4P-ECAP+CR condition. It is known that the amount of "m" and its changes influence the total elongation, and therefore can be a reason for the observed changes in elongation (Fig. 4). As obvious, the strain rate sensitivity exhibits a weak dependence of strain for heavily deformed 6061 alloy especially when ECAP and rolling are together. In other words, the strain rate sensitivity of processed by ECAP+CR sample was found to be almost constant with the applied strain. Table 3 provides a detailed summary of the hot deformation of the alloy in different conditions. As shown in Table 3, different parameters such as SPD method and tensile test condition can have significant effects on the hot deformation behavior of the studied alloy. Applying higher plastic strain and smaller gauge length lead to an increase in the ductility.

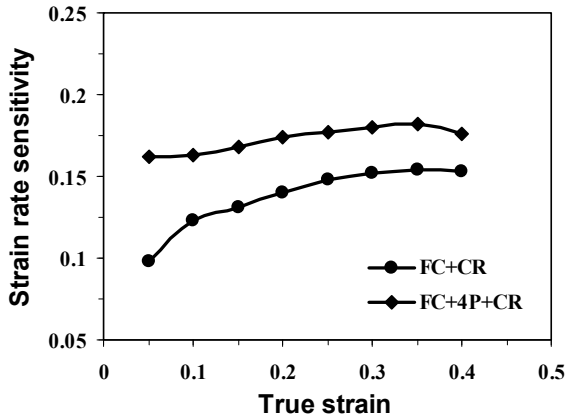

Fig. 5. Variation of strain rate sensitivity with strain.

3.2. Microstructural evolutions

3.2.1. Microscopic analysis

To confirm the changes in mechanical properties, the microstructure evolutions were characterized using LOM and TEM techniques. Figure 6a shows the microstructures of un-deformed AA6061 in the full annealing condition. The microstructure of the studied alloy before plastic deformation was consisted of coarse grains and scattered precipitates. In addition, the average size of equiaxed grains is approximately

20µm. The influence of strain on the microstructure of processed by ECAP specimens is presented in Fig. 6 (b to d). As the strain is increased from 0.76 to 2.28, the equiaxed grains become more prevalent.

Table 3. A comparison of the maximum elongation of SPD-processed AA6061-O (FC: Furnace Cooled) in high temperature.

Severe Plastic Deformation			Tensile Test					
Process	T (^{o}C)	ε (%)	$\dot{\varepsilon}$ (s^{-1})	Gl (mm)	$l/A^{1/2}$	YS (MPa)	UTS (MPa)	El (%)
MAC/F +CR [32]	RT	5.75	1×10^{-4}	10	3.48	347	360	-
ECAP [32]	RT	4.2	1×10^{-4}	10	3.48	280	300	-
ARB [33]	RT	6.3	8.3×10^{-4}	10	4.47	-	360	5
ECAP [34]	RT	6	3.3×10^{-4}	5	2.04	280	305	16
ECAP [18]	RT	8	9×10^{-4}	18	5.29[a]	-	340	5
ECAP [18]	RT	16	9×10^{-4}	18	5.29[a]	-	300	5
HRDSR [35]	120	1.2	5×10^{-4}	5	-	277	301	6.8
ECAP [36]	70	0.9	5×10^{-4}	8.8	1[a]	205	212	18
ECAP [36]	125	0.9	5×10^{-4}	8.8	1[a]	197	208	22
CR [This study]	RT	2.2	4×10^{-4}	31	10.33	250	269	3.12
ECAP+CR [This study]	RT	5.24	4×10^{-4}	31	10.33	340	384	4.11

A: the initial cross section; RT: Room Temperature; a: Cylindrical tensile specimens

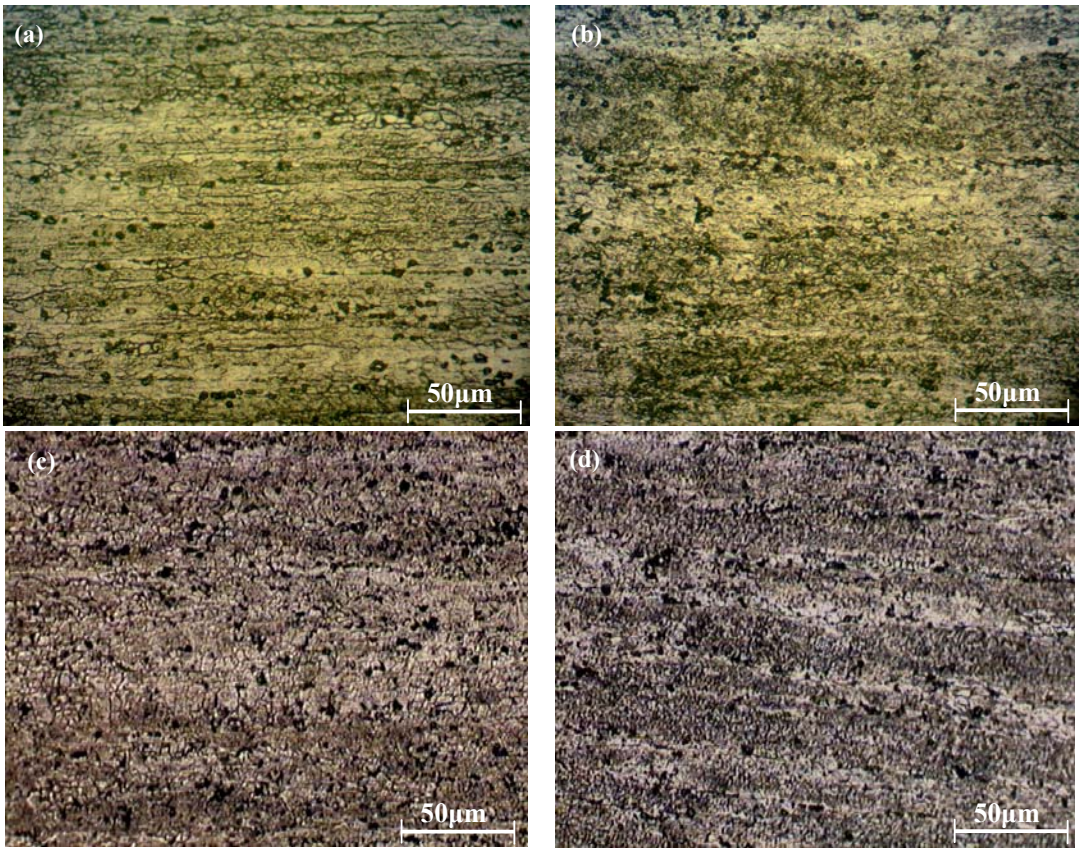

Fig. 6. LOM study of microstructure of the 6061-Al alloy, (a) before deformation and after ECApressing at: (b) 1 pass (FC+1P), (c) 2 pass (FC+2P) and (d) 3 pass (FC+3P).

During the ECAP process, the work piece is subjected to severe plastic deformation resulting in severe shear strains when passing repeatedly through the die corner. The bands of fine subgrains are usually formed along the shear direction at the first pass of pressing. This is due to the pure shear which is the characteristics of deformation by ECAP. When applying more ECAP passes, the subgrain bands are

generally divided into 3-dimensionally equiaxed ultrafine grains with high angle boundary [27]. The microstructure of the work piece after 1, 2 and 3 passes of ECAP has the average grain size of about 14, 9 μm and 4 μm, respectively. After the forth pass, the totally applied strain is about 3.1 leading to the final grain size of 1 μm (Fig. 7a). Besides, the volume fraction of smaller grains is increased resulting in the intensity of shear-band zones in the structure. In other words, the higher the employed strain is, the greater the structure homogeneity. This is an agreement with the past works on ECAP processing Al6061 alloy. It was reported [21,28] that for the sample with the initial grain size of 75 μm, after performing 4, 8 and 12 passes of ECAP, the average grain sizes of about 3.8, 1 and 0.8 μm were obtained, respectively. It is found that the initial grain size has significant effect on the final grain size after ECAP processing. The improvement in the mechanical properties of the processed by ECAP Al6061 can be also explained by the grain size effect. Comparing Figs. 7a, 7c and 7e, the grain/subgrain refinement in the ECAP plus processed by CR sample (370 nm) is more pronounced than in processed by 4P-ECAP (860 nm) and cold rolled (700 nm) samples, presumably due to applying higher plastic strain. According to Figs. 7b, 7d and 7f, the ring-like shape of the SAED pattern of the processed by ECAP (4P)+CR sample indicates the development of higher number of very small subgrains with advancing the disorientation angle between subgrain boundaries.

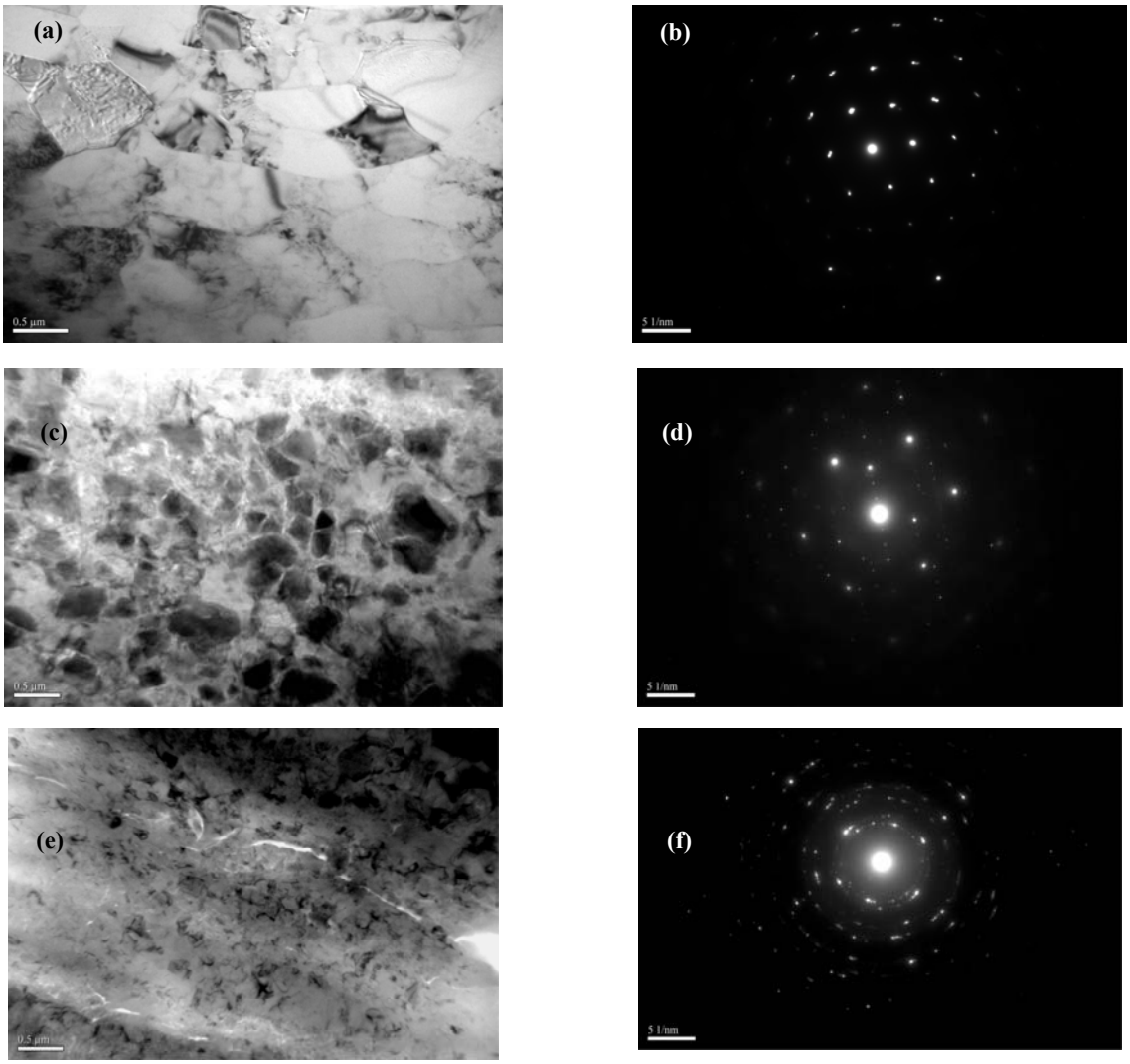

Fig. 7. TEM micrographs and the selected area diffraction patterns (SAED) of the samples of (a,b) FC+4P, (c,d) FC+CR and (e,f) FC+4P+CR.

3.2.2. X-ray diffraction analysis

Using X-ray diffraction (XRD) technique, the microstructural evolutions were characterized in terms of the presence of second phases, the shifting in peak, maximum peak intensity changes, broadening peak and the variation of lattice parameter. They are necessary to study of the effect of two SPDs method on the structure. The X-ray diffraction (XRD) patterns of the non-deformed and deformed samples are shown in Fig. 8. According to Fig. 8a, different precipitates such as Mg_2Si and AlCuMgSi are revealed for as-received and processed by ECAP samples. Most of these precipitates have already formed during the slow cooling of homogenizing treatment. A small intensity peak for these precipitates can be correlated to low amount of these phases. Figure 8b compares the shifting of XRD peaks obtained at three different conditions, i.e. as-received, processed by ECAP, cold rolled and combination of ECAP plus CR. All the peaks corresponding to the two planes ((111) and (200)) regarding the processed by CR and processed by ECAP+CR samples are shifting to left when compared to those of as-received alloy. Referring to Fig. 8b, the deviation of the peaks from initial state (as-received sample) rises with increasing the plastic strain especially in case of processed by ECAP+CR specimen. For (111) and (200) plane, it is 0.56 and 0.7 degrees for un-deformed and the processed by SPD samples, respectively. The shifts in XRD peaks are attributed to the enhanced strain [29] and consequently residual stresses in the material [30]. It is found that decreasing of 2Θ due to applying high plastic strain causes an increase in the lattice parameter. Also in reference [31], it is reported that the hypothesis of particle dissolution and the consequent solute redistribution in the matrix, together with severe plastic deformation effect (high density of dislocations and point defects) could explain the increment of lattice parameter. The variations in the peak intensity of the samples in the different conditions are shown in Fig. 8c. It is of interest that for a given condition, the maximum intensities of XRD patterns are pertaining to different planes. For example, although the largest peak for as-received sample is based on the (200), the (111) is dominant for processed by ECAP (4P) condition. It is reported that the increase in the (111) peak intensity after 3P-ECAP indicates the crystallographic restructuring of {111} plane which is the major slip plane of FCC metals [32]. Another interesting point is a significant reduction of the peak intensity for processed by CR and processed by ECAP (4P)+CR samples when compared to initial and processed by ECAP conditions. It should be noted that the peak intensities of (111) and (200) planes are surprisingly identical when ECAP and CR are carried out. These results can be due to the formation of different textures, the fluctuations in the dislocation densities and the formation of ultra fine grains (UFGs) during ECAP and CR [32]. Figure 8d illustrates the full width of half-maximum of X-ray peaks (FWHM) from the samples having different high plastic deformation. However, they are almost similar for the case of rolled samples on (111) plane. It can be seen that an increase in the widths of X-ray peaks were observed which indicate the enhancement of internal/lattice strain [33], the development of fine subgrains [34], the grain refinement [35], increase in the defect density and higher lattice distortion [36]. furthermore, in HPT method, broadening of the diffraction pattern has been attributed to the formation of an ultra fine-grained structure and residual stresses [37].

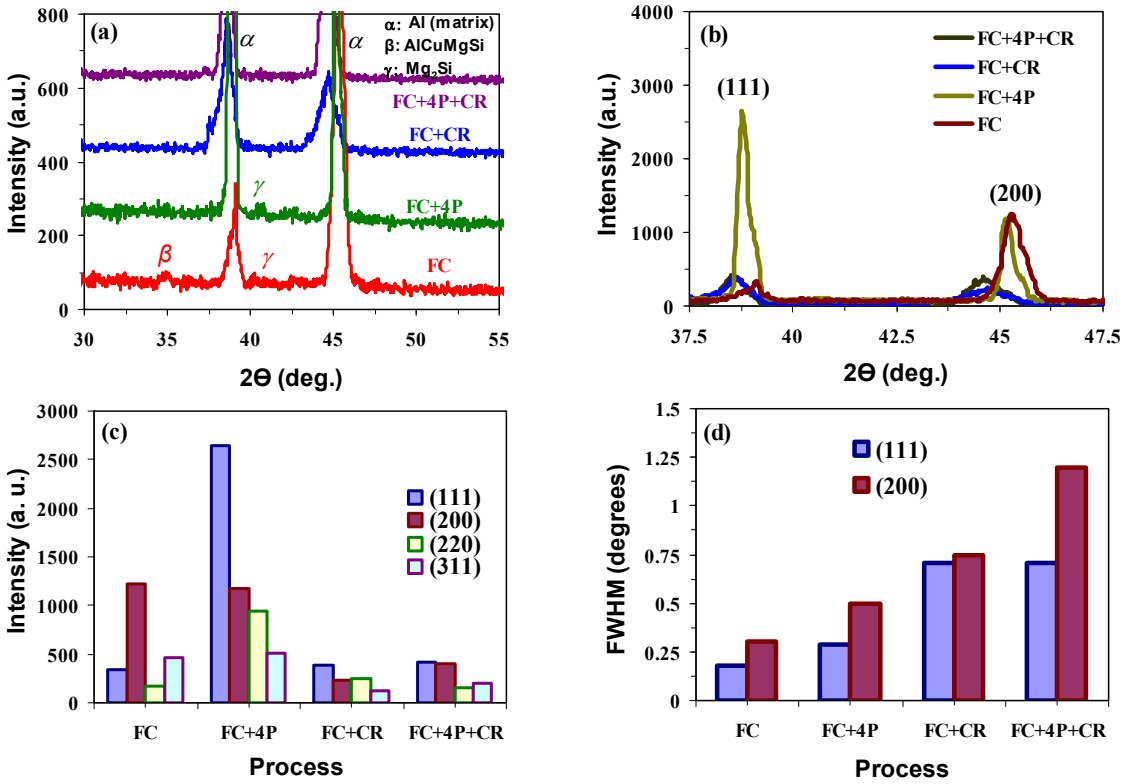

Fig. 8. (a) XRD pattern for the undeformed and deformed sample, (b) the peak position of two planes, (c) the peak intensity for the XRD experiments, (d) Peak width data (FWHM, full width half maximum).

4. Discussion

4.1. Effect of ECAP and Subsequent Cold Rolling on Cold Formability

According to the stress-strain curves (Fig. 1), the immediate appearance of the stress peak at very low strains indicates the low work hardening of processed by ECAP specimen. However, the dominate shear strain in the ECAP process led to the extension of post-necking strain in the stress–strain curves. In fact, the stress-strain curves do not exhibit strain hardening; i.e. the flow stress does not increase with strain. By contrast, the combined ECAP+CR process resulted in an increase in the work hardening, though a decrease in the post-necking strain was observed. In other words, the combination of pure shear strain in ECAP and true strain in rolling can improve both ductility and strength. According to Fig. 2, the ratio of yield stress to ultimate tensile stress can be a good criterion for work-hardening studies. An increase in this ratio with increasing the number of ECAP passes or the applied strain indicates that the work hardening is decreased. This is the typical characteristics of UFG materials processed by severe plastic deformation attributed to their low dislocation storage capability [38]. However, the present results indicate that, comparing to processed by ECAP case, the combination of ECAP and CR resulted in an increase in the work hardening. In fact, by applying two different SPD techniques, both the strength and ductility are enhanced. As the SFE of aluminum alloys is high, the observed behavior can be due to the fast dynamic-recovery rate in case of high SFE materials. This behavior is usually observed in the un-processed by SPD alloys at later stage of deformation. Dynamic-recovery rate increases with the increase in dislocation density because the probability of dynamic recovery increases as the distance between dislocations decreases [23]. In addition, the atomic-scale simulations regarding the specimens subjected to large/severe grains revealed more detailed information about the dislocation processes that are consistent

with the behavior expected in coarse-grained materials. During the flow of material, a great variety of dislocation activities are observed. For example, according to the simulation results, the new dislocations are generated at the grain boundaries, glide through grains, and are then absorbed at other grain boundaries. At these grains, the main sources of new dislocations are the grain boundaries rather than, for example, Frank-Read sources in the grain interiors. The dislocations sometimes intersect or get trapped by stacking faults. However, the dislocation interactions do not lead to dislocation tangles and permanent immobilization of the dislocations, though rarely a few Lomer-Cottrell locks are created and destroyed soon after. This result is in line with the stress-strain curves that do not exhibit strain hardening; i.e. the flow stress does not increase with strain. Thus, in case of nanocrystalline metals, the lack of strain hardening is believed to be responsible for their low ductility [39].

4.2. The Combination effect of ECAP and subsequent CR on hot formability

Analyzing the results reported in the present work shows that the hot deformation behavior of processed by ECAP+CR sample is different from that of other samples. The question is whether the changes in deformation mechanism are influenced by microstructural evolutions or not and also what the reason is for shifting the highest elongation (obtained at the lowest strain rates) to even higher amount after applying the cold rolling to processed by ECAP samples. To find the answer, at first the hot deformation behavior is studied, followed by investigating the microstructural evolutions. Referring to Figures 3 and 4, the unusual strain rate dependence of hot ductility on the different conditions of processed by SPD samples suggests a change in deformation mechanism. When ECAP and CR are combined together, the strain rate sensitivity always is higher than CR alone. The lower strain-rate sensitivity caused by only rolling process is due to the more rapid necking (see Fig. 5). It is well known that the high coefficient of strain-rate sensitivity enhances the post-necking elongation and leads to higher ductility or superplasticity [40, 41]. Thus, higher elongations can be attributed to higher amount of strain-rate sensitivity. Therefore, it is clear why the ductility of processed by ECAP+CR sample is always higher than other cases (Fig. 4). The plot in Fig. 8a indicates that the peak intensities of the precipitates are disappeared by applying heavy cold rolling. The absence of the second phases can be attributed to dissolution of the precipitates due to high level of plastic deformation. This finding is in consistent with the results reported in References [42] and [31]. Thus XRD results indicate that the influence of second phases is reduced by increasing strain. In fact, hot deformation behavior of deformed 6061Al alloy can not be influenced by precipitates significantly. On the other hand, according to the results of TEM (Fig. 7) and XRD pattern (Fig. 8), the formation of ultra fine grains (UFGs) and increasing the defect densities (dislocations) in case of ECAP+CR can be the reasons of observed changes in deformation mechanism. Also, it was reported [14] that the higher strains associated with additional rolling after ECAP is expected to enhance the high angle boundaries compared to ECAP only. Since high angle boundaries are a prerequisite for the occurrence of grain boundary sliding and superplastic flow [43], it is clearly evident that 4 passes of ECAP followed by subsequent rolling induce higher elongation comparing to other samples. Besides, the subsequent rolling after ECAP leads to achieving high ductility at higher strain rates (Fig. 4). It can be concluded that the above findings are due to an increase in the fraction of high angle boundaries [43]. Similar results are reported in previous study for the modified AA5154 alloy [14], AA7034 alloy [43] and the severely deformed Al–Mg–Sc–Zr alloy [44]. Therefore, applying the ECAP followed by CR processing has the advantages such as achieving higher superplasticity comparing to only ECAP or CR. In accordance with the references [24, 45, 46], ECAP processing and subsequent rolling lead to the improvement of the superplastic properties of aluminum alloys comparing to the ECAP or CR only.

4. Conclusion

For industrial applications, large workpieces of AA6061 were subjected to a combined process consisting of ECAP followed by cold rolling. The yield strength and the ultimate tensile strength were increased with increasing the number of ECAP passes. The improvement in the mechanical properties of the alloy can be explained by the grain size effect. Subsequent higher strains applied by rolling after ECAP resulted in a considerable improvement of mechanical properties at hot and cold temperatures. Considering the mechanical properties and microstructure evolution in different processing conditions, one can conclude that the best cold/hot deformation behavior for the alloy used in this research is the combination of $4P_{ECAP}$ and cold rolling processes. Therefore, the combination of two SPD techniques can be a practical method to fabricate the large workpieces for industrial applications.

Acknowledgement: The authors would like to acknowledge the help of Professor Reza Mahmudi and the staff of formability laboratory for their contribution in this work. The authors also thank to Mr. S.A. Motaei and Mr. Haghani for running the ECAP and Rolling system.

5. References

1. M.J. Zehetbauer and Y.T. Zhu, Bulk nanostructure, (2009) Wiley-Vch.
2. R.Z. Valiev and T.G. Langdon, Principles of equal-channel angular pressing as a processing tool for grain refinement, *Progress Material Science*, 51 (2006) 881-981.
3. R.Z. Valiev and T.G. Langdon, Achieving exceptional grain refinement through severe plastic deformation: New approaches for improving the processing technology, *Metallurgical and Materials Transactions A*, 42 (2011) 2942-2951.
4. R.Z. Valiev, Nanostructuring of metals by severe plastic deformation for advanced properties, *Nature Material*, 3 (2004) 511-516.
5. S. Ferrasse, V.M. Segal, F. Alford, J. Kardokus and S. Strothers, Scale up and application of equal-channel angular extrusion for the electronics and aerospace industries, *Materials Science and Engineering A*, 493 (2008) 130-140.
6. M. Vaseghi, A. Karimi Taheri, S.I. Hong and H.S. Kim, Dynamic ageing and the mechanical response of Al–Mg–Si alloy through equal channel angular pressing, *Material and Design*, 31 (2010) 4076-4082.
7. S.K. Panigrahi and R. Jayaganthan, Development of ultrafine grained Al–Mg–Si alloy with enhanced strength and ductility, *Journal of Alloys and Compounds*, 470 (2009) 285-288.
8. A. Loucif, R.B. Figueiredob, T. Baudin, F. Brisset and T.G. Langdon, Microstructural evolution in an Al-6061 alloy processed by high-pressure torsion, *Materials Science and Engineering A*, 527 (2010) 4864-4869.
9. E.C. Moreno-Valle, I. Sabirov, M.T. Perez-Prado, M.Y. Murashkin, E.V. Bobruk and R.Z. Valiev, Effect of the grain refinement via severe plastic deformation on strength properties and deformation behavior of an Al6061 alloy at room and cryogenic temperatures, *Material Letter*, 65 (2011) 2917-2919.
10. M.R. Rezaei, M.R. Toroghinejad and F. Ashrafizadeh, Effects of ARB and ageing processes on mechanical properties and microstructure of 6061 aluminum alloy, *Journal of Materials Processing Technology*, 211 (2011) 1184-1190.
11. A.A. Mogucheva and R.O. Kaibyshev, Structure and properties of aluminum alloy 1421 after equal-channel angular pressing and isothermal rolling, The Physics of Metals and Metallography, 106 (2008) 424–433.
12. S. Ferrasse, V.M. Segal and E. Alford, Effect of additional processing on texture evolution of Al0.5Cu alloy processed by equal channel angular extrusion (ECAE), *Materials Science and Engineering A*, 372 (2004) 44-55.

13. P.K. Chaudhury, B. Cherukuri and R. Srinivasan, Scaling up of equal-channel angular pressing and its effect on mechanical properties, microstructure, and hot workability of AA 6061, *Materials Science and Engineering A*, 410–411 (2005) 316–318.
14. K.T. Park, H.J. Lee, C.S. Lee, W.J. Nam, D.H. Shin, Enhancement of high strain rate superplastic elongation of a modified 5154 Al by subsequent rolling after equal channel angular pressing, Scripta Materialia, 51, (2004) 479-483.
15. A.R. Eivani and A. Karimi Taheri, Effective strain based on shear and principal strains in equal channel angular extrusion with outer curved corner, *Computational Materials Science*, 41 (2008) 409–419.
16. M. Kamachi, M. Furukawa, Z. Horita and T.G. Langdon, Equal-channel angular pressing using plate samples, *Materials Science and Engineering*, A361 (2003) 258–266.
17. ASTM E8/E8M−13a, American Society for Testing and Materials Standard Test Methods for Tension Testing of Metallic Materials, (2013) 1–28.
18. B. Cherukuri, T.S. Nedkova and R. Srinivasan, A comparison of the properties of SPD-processed AA-6061 by equal-channel angular pressing, multi-axial compressions/forgings and accumulative roll bonding, *Materials Science and Engineering* A 410–411 (2005) 394–397.
19. S.H. Lee, Y. Saito, T. Sakai and H. Utsunomiya, Accumulative roll bonding of pure copper and IF steel, *Materials Science and Engineering A*, 325 (2002) 228-235.
20. Z. Horita, T. Fujinami, M. Nemoto and T. G. Langdon, Equal-channel angular pressing of commercial aluminum alloys: Grain refinement, thermal stability and tensile properties, *Metallurgical and Materials Transactions A*, 31 (2000) 691-701.
21. Y.W. Tham, M.W. Fu, H.H. Hng, Q.X. Pei and K.B. Lim, Microstructure and properties of Al-6061 alloy by equal channel angular extrusion for 16 passes, *Materials and Manufacturing Processes*, 22 (2007) 819–824.
22. W.J. Kim, J.Y.Wang, S.O. Choi, H.J. Choi and H.T. Sohn, Synthesis of ultra high strength Al–Mg–Si alloy sheets by differential speed rolling, *Materials Science and Engineering A*, 520 (2009) 23–28.
23. J.K. Kim, H.K. Kim, J.W. Park, W.J. Kim, Large enhancement in mechanical properties of the 6061 Al alloys after a single pressing by ECAP, *Scripta Materialia*, 53 (2005) 1207–1211.
24. H. Akamatsu, T. Fujinami, Z. Horita, T.G. Langdon, Influence of rolling on the superplastic behavior of an Al-Mg-Sc alloy after ECAP, *Scripta Materialia*, 44 (2001) 759-764.
25. K.T. Park, H.J. Lee, Ch.S. Lee and D.H. Shin, Effect of post-rolling after ECAP on deformation behavior of processed by ECAP Commercial Al–Mg Alloy at 723K, *Materials Science and Engineering A*, 393 (2005) 118–124.
26. W.J. Kim and S.J. Yoo, Enhanced ductility and deformation mechanisms of ultrafinegrained Al–Mg–Si alloy in sheet form at warm temperatures, *Scripta Material*, 61 (2009) 125-128.
27. K.T. Park, H.J. Kwon, W.J. Kim and Y.S. Kim, Microstructural characteristics and thermal stability of ultrafine grained 6061 Al alloy fabricated by accumulative roll bonding process, *Materials Science and Engineering A*, 316 (2001) 145–152.
28. M.W. Fu, Y.W. Tham, H.H. Hng and K.B. Lim, The grain refinement of Al-6061 via ECAE processing: Deformation behavior, microstructure and property, *Materials Science and Engineering A*, 526 (2009) 84-92.
29. B. Gopi, N. Naga Krishna, K. Venkateswarlu and K. Sivaprasad, Influence of rolling temperature on microstructure and mechanical properties of cryorolled Al-Mg-Si alloy, *World Academy of Science, Engineering and Technology*, 61 (2012) 731-735.
30. L. Kurmanaeva, Yu. Ivanisenko, J. Markmanna, C. Kübel, A. Chuvilin, S. Doyle, R.Z. Valiev and H.J. Fecht, Grain refinement and mechanical properties in ultrafine grained Pd and Pd–Ag alloys produced by HPT, *Materials Science and Engineering*, A 527 (2010) 1776–1783.
31. E. Cerri and P. Leo, Influence of severe plastic deformation on aging of Al–Mg–Si alloys, *Materials Science and Engineering A*, 410–411 (2005) 226–229.

32. E. Tan, A.A. Kibar and C.H. Gür, Mechanical and microstructural characterization of 6061 aluminum alloy strips severely deformed by dissimilar channel angular pressing, *Materials Characterization*, 62 (2011) 391 – 397.
33. Z. Lee, F. Zhou, R.Z. Valiev, E.J. Lavernia and S.R. Nutt, Microstructure and microhardness of cryomilled bulk nanocrystalline Al–7.5%Mg alloy consolidated by high pressure torsion, *Scripta Materialia*, 51 (2004) 209–214.
34. M. Weiss, A.S. Taylor, P.D. Hodgson and N. Stanford, Strength and biaxial formability of cryo-rolled 2024 aluminium subject to concurrent recovery and precipitation, *Acta Materialia* 61 (2013) 5278-5289.
35. A.A. Mazilkin et al. Softening of nanostructured Al–Zn and Al–Mg alloys after severe plastic deformation, *Acta Materialia*, 54 (2006) 3933–3939.
36. A.A. Mazilkin, B.B. Straumal, E. Rabkin, B. Baretzky, S. Enders, S.G. Protasova, O.A. Kogtenkova and R.Z. Valiev, Grain refinement and properties of pure Ti processed by warm ECAP and cold rolling, *Materials Science and Engineering A* 343 (2003) 43-50.
37. H. Ferkel, Y. Estrin, C. Blawert and R.Z. Valiev, RF nitriding of severely deformed Armco iron and St2K50, *Surface and Coatings Technology*, 173 –174 (2003) 1164–1170.
38. Y.H. Zhao, Y.Z. Guo, Q. Wei, A.M. Dangelewicz, C. Xu, Y.T. Zhu, T.G. Langdon, Y.Z. Zhou and E.J. Lavernia, Influence of specimen dimensions on the tensile behavior of ultrafine-grained Cu, *Scripta Materialia*, 59 (2008) 627–630.
39. J. Schiøtz, F. D. Di Tolla and K. W. Jacobsen, Softening of nanocrystalline metals at very small grain sizes, *Nature*, 391 (1998) 561–563.
40. G.E. Dieter, H.A. Kuhn and S.L. Semiatin, Handbook of Workability and Process Design, ASM International, first edition, (2003).
41. H.J. McQueen, S. Spigarelli, M.E. Kassner and E. Evangelista, Hot *deformation and processing of aluminum alloys*, first edition, Taylor & Francis Group (2011).
42. V.L. Niranjani, K.C. Hari Kumar and V. Subramanya Sarma, Development of high strength Al–Mg–Si AA6061 alloy through cold rolling and Ageing, *Materials Science and Engineering A*, 515 (2009) 169–174
43. Ch. Xu, M. Furukawa, Z. Horita and T.G. Langdon, Using ECAP to achieve grain refinement, precipitate fragmentation and high strain rate superplasticity in a spraycast aluminum alloy, *Acta Materialia*, 51 (2003) 6139–6149.
44. E. Avtokratova, O. Sitdikov, M. Markushev and R. Mulyukov, Extraordinary high-strain rate superplasticity of severely deformed Al–Mg–Sc–Zr alloy, *Materials Science and Engineering A*, 538 (2012) 386– 390.
45. K.T. Park, H.J. Lee, Ch.S. Lee and D.H. Shin, Effect of post-rolling after ECAP on deformation behavior of processed by ECAP commercial Al–Mg alloy at 723K, *Materials Science and Engineering A*, 393 (2005) 118–124.
46. A.A. Mogucheva and R.O. Kaibyshev, Structure and properties of aluminum alloy 1421 after equal-channel angular pressing and isothermal rolling, *The Physics of Metals and Metallography*, 106 (2008) 424–433.